Journal of Materials Chemistry A

PAPER

View Article Online
View Journal

Cite this: DOI: 10.1039/d5ta09175f

Chain-length-selective adsorption governs diffusion-limited dendrite growth mode in battery electrodes

Aakriti Aggarwal,[a] Wenrui Chai,[b] Graeme Henkelman [b] and Kent J. X. Zheng [*acd]

Growth of classical dendrites in metal anodes represents a far-from-equilibrium, diffusion-limited crystallization process that critically impacts the safety and performance of energy storage systems. Zn—a promising aqueous anode material—exhibits two distinct modes: continuous growth (CG), where a few crystallographically guided dendrites propagate rapidly, and independent nucleation (IN), where numerous smaller, randomly oriented dendrites form with slower propagation. Here we show that ethylene glycol-derived additives, $HO–(CH_2CH_2O)_n–H$, can reliably shift growth from CG to IN. Using *operando* tools including optical visualization, electrochemical impedance spectroscopy, and quartz crystal microbalance, we resolve the kinetic and interfacial origins of this transition. The effect is highly chain-length dependent: PEG-400 ($n \approx 9$) achieves the most efficient CG → IN shift with a threshold of 0.001 wt% (10 ppm), while shorter or longer chains require ~1 wt%, and no transition occurs for $n \leq 3$ at all. Experimental measurements and quantum-chemical analysis reveals that the transition arises from two coupled processes: adsorption of PEG molecules at the electrode surface, and coordination with Zn adatoms and Zn^{2+} cations, which destabilize continuous growth pathways and favor repeated independent nucleation. Importantly, the shift from CG to IN reduces dendrite propagation velocity by a factor of 6. These findings establish molecular-level design rules for engineering task-specific organic molecules to control far-from-equilibrium crystallization, with direct implications for high-power batteries and electrochemical synthesis.

Received 11th November 2025
Accepted 24th February 2026

DOI: 10.1039/d5ta09175f

rsc.li/materials-a

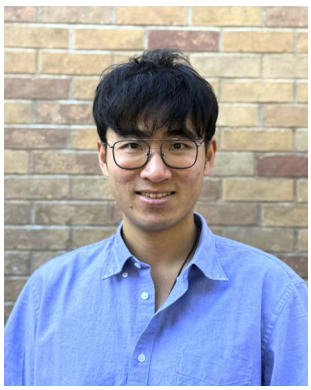

Kent J. X. Zheng

Kent Zheng is an Assistant Professor in the McKetta Department of Chemical Engineering at The University of Texas at Austin. He joined UT Austin in Spring 2024, following his postdoctoral training in the Department of Physics at MIT. He currently serves as an Associate Editor for ECS Advances (2024-present), appointed by The Electrochemical Society. As of March 2026, he has co-authored more than 80 peer-reviewed publications. His honors include the Early Career Award from the ECS Electrodeposition Division, the MRS Buck Robinson Award for Renewable Energy, and recognition as a Forbes 30 Under 30 honoree (2025).

Crystallization under far-from-equilibrium conditions, driven by steep gradients in temperature or concentration, remains a fundamental scientific challenge with broad industrial relevance.[1–3] Such interfacial instabilities often give rise to dendritic growth, characterized by highly ramified, self-similar fractal geometries. In metallurgy, aggressive formation of coarse thermal dendrites are well known to degrade the mechanical properties of solidified alloys.[4,5] In batteries, dendrites form under fast-charging conditions when rapid ion reduction ($M_{(solution)}^{n+} + ne^- \rightarrow M_{(solid)}$) depletes local ion concentration, establishing sharp gradients that trigger self-reinforcing propagation into the bulk electrolyte.[6–8] This behavior is commonly rationalized by the relative rates of ion transport and electrochemical reaction: when the reaction kinetics (exchange current density, j_0) greatly exceeds the transport-limits (j_{lim}), the electrode surface experiences severe ion depletion and dendrite initiation.[9,10] It is further revealed that the crystallographic anisotropy of the depositing metal strongly influences dendrite evolution.[3,11,12] For high-anisotropy

[a]Department of Chemical Engineering, University of Texas at Austin, Austin, Texas 78712, USA. E-mail: kentz@utexas.edu
[b]Department of Chemistry, University of Texas, Austin, Texas 78712, USA
[c]Texas Materials Institute, University of Texas at Austin, Austin, Texas 78712, USA
[d]Bard Center for Electrochemistry, University of Texas at Austin, Austin, Texas 78712, USA

metals such as hexagonal close-packed (HCP) Zn, once a dendrite nucleates it propagates rapidly along lattice-preferred directions, producing highly localized filaments that accelerate short-circuit failure.[11]

Organic species have long been recognized as effective modulators of electrodeposition.[13–15] Among them, ethylene-glycol-derived (EG) molecules—ranging from short oligomers to long-chain polymers—are widely reported to enhance the interfacial stability of metal deposition in aqueous electrolytes through surface adsorption.[8,16–19] While surface adsorption is well established in the literature, the precise mechanisms by which it governs the electrodeposition process—particularly, in the mass-transport-limited dendritic regime—remain an open area of investigation; with few exceptions,[8,20] most prior reports have focused on the influence of EG-derived molecules at electrodeposition rates well below the limiting current density, where classical dendritic growth is not expected. Several mechanisms have been proposed, including suppression of electrokinetics—as evidenced by significant reduction in j_0—that slows ion consumption[8,21,22] and modulation of viscoelastic properties that dampen electroconvection.[23,24] This motivated our work to specifically probe the impact of trace organic species on electrodeposition in the diffusion-limited regime, opening new opportunities for enabling ultrafast charging. Our recent results reveal that PEG-400 can fundamentally alter the geometry of Zn dendrites formed under classical mass-diffusion-limited conditions.[11] In the absence of PEG-400, Zn growth is dominated by a small number of colossal dendrites that, once nucleated, undergo continuous growth (Mode I: CG) along crystallographically preferred directions. This highly localized tip growth produces extremely rapid propagation rates ($\sim 6 \times 10^1$ μm s^{-1}) and is particularly detrimental to stability. By contrast, in the presence of 1 wt% PEG-400, growth shifts to independent nucleation (Mode II: IN), characterized by a large number of smaller dendrites forming without orientational correlation. This morphology remarkably slows the effective dendrite-front propagation speed, by *a* factor of 4. Together, these earlier observations highlight the complex role of EG-derived organics in aqueous electrodeposition and their profound influence on morphological evolution under far-from-equilibrium conditions.

Motivated by the decisive role of a small amount (1 wt%) of PEG-400 in shifting Zn dendrite growth from Mode I: CG to Mode II: IN, this work employs *operando* optical visualization, electrochemical impedance spectroscopy (EIS), quartz crystal microbalance (QCM), and nuclear magnetic resonance (NMR) to elucidate the governing mechanisms of ethylene-glycol-derived additives [HO–$(CH_2CH_2O)_n$–H] in shifting the dendritic growth mode. *Operando* microscopy establishes the primary trends: the CG → IN transition is absent for short chains ($n \leq 3$), begins to appear at $n \geq 4$ with a concentration threshold C_t of ~1 wt%, and reaches maximum efficiency at $n \approx 9$ (PEG-400), where the threshold is as low as 0.001 wt%! For longer chains ($n > 9$), the transition remains possible but requires progressively higher concentrations. The threshold concentration (C_t) is defined as the highest measured polymer additive concentration at which independent nucleation (IN) growth mode is observed before transition to continuous growth (CG) mode upon dilution. QCM measurements reveal that adsorbed mass on the Zn surface increases monotonically with chain length, explaining why short oligomers cannot induce the transition. However, this trend cannot account for the reduced efficiency observed for very long chains. NMR measurements provide complementary insight, showing the largest salt-induced peak shift at $n \approx 9$, indicative of the strongest PEG–Zn^{2+} interaction. Together, these results suggest that the growth-mode transition requires two conditions: (i) effective adsorption of the additive on the electrode and (ii) strong interaction with Zn species. This dual criterion explains the exceptional efficiency of PEG-400. Density functional theory (DFT) calculations further support this model, showing that adsorbed species stabilize surface adatoms, suggesting suppression of continuous tip growth and promoting independent nucleation. These findings demonstrate how molecular-level physicochemical interactions dictate macro-scale morphological evolution under far-from-equilibrium conditions, offering design rules for task-specific molecular engineering in electrochemical deposition and energy storage.

Results and discussion

Operando mapping of critical transitions in dendrite growth modes

Fig. 1 presents the dendrite morphological modes in the presence and absence of EG-derived species in the electrolyte, characterized by *operando* optical visualization, SEM, and laser profilometry. Details of the experimental setup and electrochemical protocol are provided in Fig. S1 and S2.[25] In concentrated $ZnCl_2$ aqueous electrolyte without EG-derived species, dendritic growth is dominated by a small number of primary dendrites with parallel branches and correlated six-fold geometrical features, indicative of continuous growth along fast-propagating directions (*e.g.*, $[100]_{Zn}$) defined by the HCP lattice (Fig. 1a–c; Mode I: CG). By contrast, the addition of EG-derived species shifts the dendrite growth into a fundamentally different regime, producing a large number of independently nucleated Zn particles without orientational correlation (Fig. 1d–f; Mode II: IN). See Fig. S3 for detailed visualizations of the transition and Fig. S4 for a more quantitative definition of the CG and IN growth modes.

Most importantly, *operando* visualization reveals a critical dependence of the CG → IN transition on both the chain length and concentration of EG-derived species (Fig. 1g). When the chain length $n < 4$, no CG → IN transition is observed even at concentrations as high as 20 wt% (Fig. S5), indicating that EG-derived species with $n = 1$, 2, or 3 have no effect on Zn dendrite growth mode. See also Video S1 for CG growth mode observed in 1 wt% EG. By contrast, when $n \geq 4$, the CG → IN transition becomes apparent even at 1 wt% additive concentration. Notably, the lowest threshold concentration (C_t) required to induce the transition occurs at $n \approx 9$ (PEG-400); only 0.001 wt% (10 ppm) is sufficient to drive the CG → IN transition! See Video S2 for *operando* visualization. For longer chains ($n > 9$), C_t

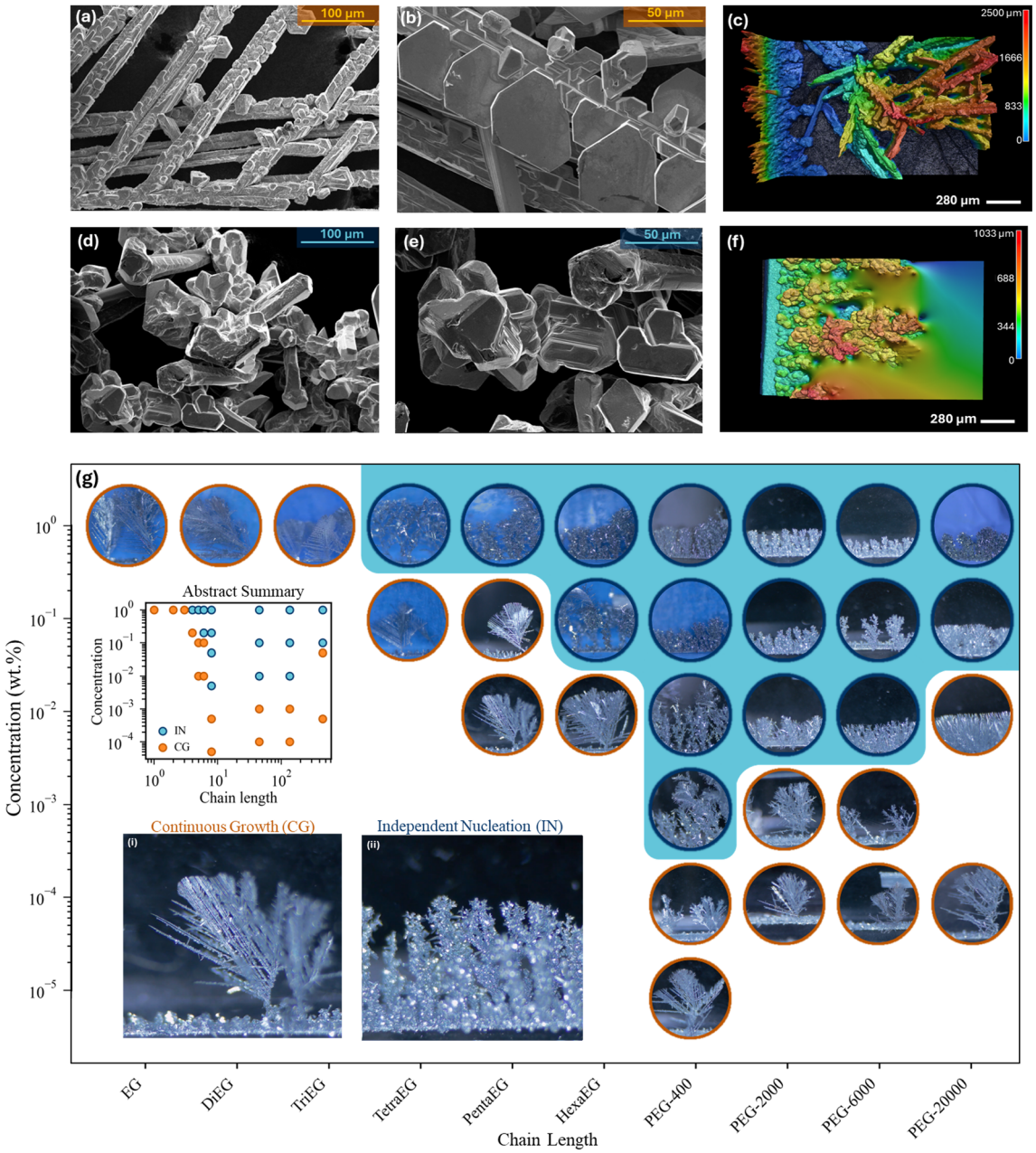

Fig. 1 Dendrite growth modes dictated by the chain length and concentration of EG-derived species. (a and b) SEM images of dendrites formed *via* continuous growth (CG) mode. (c) Laser profilometry of CG morphology. (d and e) SEM images of dendrites formed *via* independent nucleation (IN). (f) Laser profilometry of IN morphology. (g) Morphology map from in-*operando* visualization under various experimental conditions, showing either independent nucleation (IN) or continuous growth (CG) modes. The base electrolyte was 10 M $ZnCl_2$ with the concentration of polymer additives as shown. The blue region marks the IN regime; inset: simplified map with blue points highlighting IN cases: *Operando* visualization of (i) CG morphology and (ii) IN morphology.

increases, but the CG → IN transition remains robust in all situations at 1 wt%.

These two distinct dendrite growth modes lead to fundamentally different electrochemical behavior. As shown in Fig. 2a, the ohmic resistance R_Ω decreases much more rapidly with increasing areal deposition capacity (Q) in Mode I: CG (with 1 wt% EG, $n = 1$) than in Mode II: IN (with 1 wt% PEG-400), as evidenced by the Nyquist plots from the EIS measurements (Fig. 2b and S8). *Operando* optical visualization of two growth modes (Fig. 2c and d) offers a clear explanation for this observed difference in the shape of the $R_\Omega(Q)$ curve. The dendrite front propagation rate in Mode I: CG toward the counter electrode is 6 times higher than in Mode II: IN. This morphological evolution reduces the inter-electrode distance and therefore significantly lowers the measured system-level R_Ω, eventually leading to complete shorting of the cell (Fig. 2e and f). The steeper the $R_\Omega(Q)$ curve, the more efficiently the dendrite penetrates the inter-electrode gap (Fig. S9). In a given system,

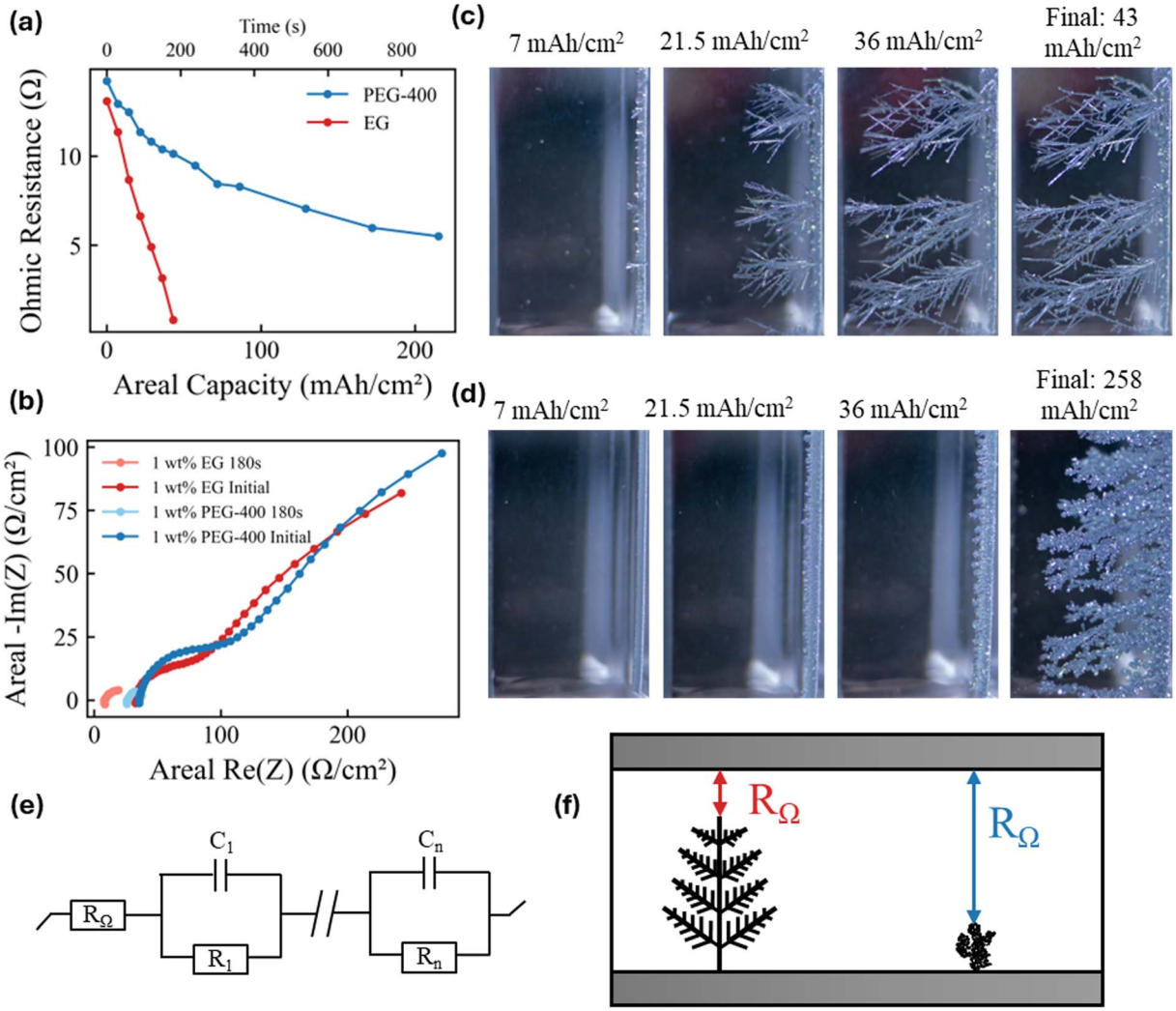

Fig. 2 Electrochemical Impedance Spectroscopy (EIS) and *Operando* optical monitoring of dendrite growth morphology. (a) Ohmic resistance R_Ω measured using EIS during constant current plating with 1 wt% EG additive as representative for CG growth and with 1 wt% PEG-400 additive as representative for IN growth. Refer to Fig. S6 and S7 for constant current *versus* constant potential protocol details. (b) Representative Nyquist plots for EIS collected for a fresh cell and after 180 s (43 mA cm^{-2}), for both electrolytes. The 1 wt% EG cell is near shorting. In-*operando* visualization of dendrite evolution at selected time intervals (c) for the EG system, and (d) PEG-400 system, respectively. (e) Equivalent circuit model used to extract ohmic resistance R_Ω. The RC elements are arbitrary elements representing different electrochemical processes in the cell. (f) Schematic comparison of showing difference in R_Ω for CG (red) and IN (blue) at the same capacity. A decrease in R_Ω indicates dendrite approach toward the counter electrode, with lower values signifying proximity to shorting (refer to Fig. S9 and S10 for further explanation).

the slope dR_Ω/dQ can thus be viewed as a quantitative measure of the dendrite's shorting tendency. To generalize this comparison across different cells, R_Ω can further be normalized and expressed as the percent change in R_Ω per unit areal capacity. This value in the Mode I: CG system (2.18) is 7 times larger than that in Mode II: IN (0.28). We attribute this stark contrast in the shape of $R_\Omega(Q)$ to the fact that dendrites in Mode I: CG preferentially extend along a few fast-growing crystallographic directions, resulting in highly localized but concerted and therefore rapid propagation. Conversely, the numerous independent Zn crystals in Mode II: IN lack orientational correlation and thus propagate toward the counter electrode in a less concerted manner. Taken together, the results in Fig. 1 and 2 demonstrate that the CG → IN transition, which profoundly affects electrochemical behavior and cell stability, is strongly governed by the molecular-level chemistry of the EG-derived species. Mechanistic insights into how these species drive the transition will be essential for guiding the rational design of electrolytes for fast-charging battery systems.

Understanding interfacial dynamics driving dendrite mode transition

Motivated by the observation that this critical transition occurs even at ppm-level concentrations of PEG-400, we hypothesize that the phenomenon is highly interfacial in nature, rather than arising from changes in bulk electrolyte properties such as conductivity or solvation structure. This hypothesis is consistent with earlier studies showing that PEG species readily

adsorb on metallic electrode surfaces such as Zn,[26] Cu,[27] and Au.[28] The possibility of bulk electrolyte properties being responsible for the CG → IN transition was explored and eliminated as discussed in Fig. S11. QCM-D measurements were performed to gain quantitative insight into the surface adsorption of EG species (Fig. S12–S15). Fig. 3a shows the mass change of the electrode when a 1 wt% PEG-400 electrolyte is flowed into the cell.[29] The return of mass change to zero after a baseline PEG-free electrolyte is re-introduced indicates that the adsorption is reversible. The difference in mass change between f3 and f5, along with a non-zero dissipation value indicates the adsorption layer is viscoelastic, refer to Note S1 for a further discussion regarding the analysis and limitations.[30] A clear positive correlation is observed between polymer chain length and the mass adsorbed on the sensor surface (Fig. 3b). This means that longer-chain polymers adsorb more extensively on the electrode surface, occupying a greater interfacial volume (Fig. S16).[31]

We now consider how adsorption can promote independent nucleation and drive the CG → IN transition. As *a* point of departure, the intrinsic continuous growth mode observed without any EG-derived species can be rationalized by classical nucleation theory. The formation of new crystals requires creating particles with high specific surface area, which imposes a higher kinetic barrier than simply extending pre-existing crystals. DFT calculations provide atomistic insight into the interaction between adsorbed EG-derived species and the growing Zn metal surface. The DFT calculations are intended to capture qualitative, comparative trends among water, ethylene glycol, and low-molecular weight PEGs, rather than to provide quantitatively accurate surface or binding energies. Fig. 4a–c shows the proposed interaction framework whereby water, ethylene glycol and PEG molecules all interact strongly with the Zn surfaces through their oxygen atom. The adsorbed molecules are likely to bind with Zn adatoms on the surface, stabilizing these otherwise highly active growth sites and thereby "passivating" the surfaces of existing crystals. This adatom passivation could make continuous growth less energetically favorable and shift the balance between continuous growth and independent nucleation, rendering the latter comparatively more favorable (Fig. 4d and e). The binding strength appears to increase with chain length, suggesting stronger adatom passivation and a greater tendency toward independent nucleation (Fig. S17). The absence of CG → IN transition in systems with $n \leq 3$ can be understood in terms of weaker adatom passivation; when passivation is insufficient, continuous growth dominates over independent nucleation.

While we can now rationalize the absence of the CG → IN transition at short chain lengths, it is less straightforward why the threshold concentration C_t reaches its minimum at $n \approx 9$

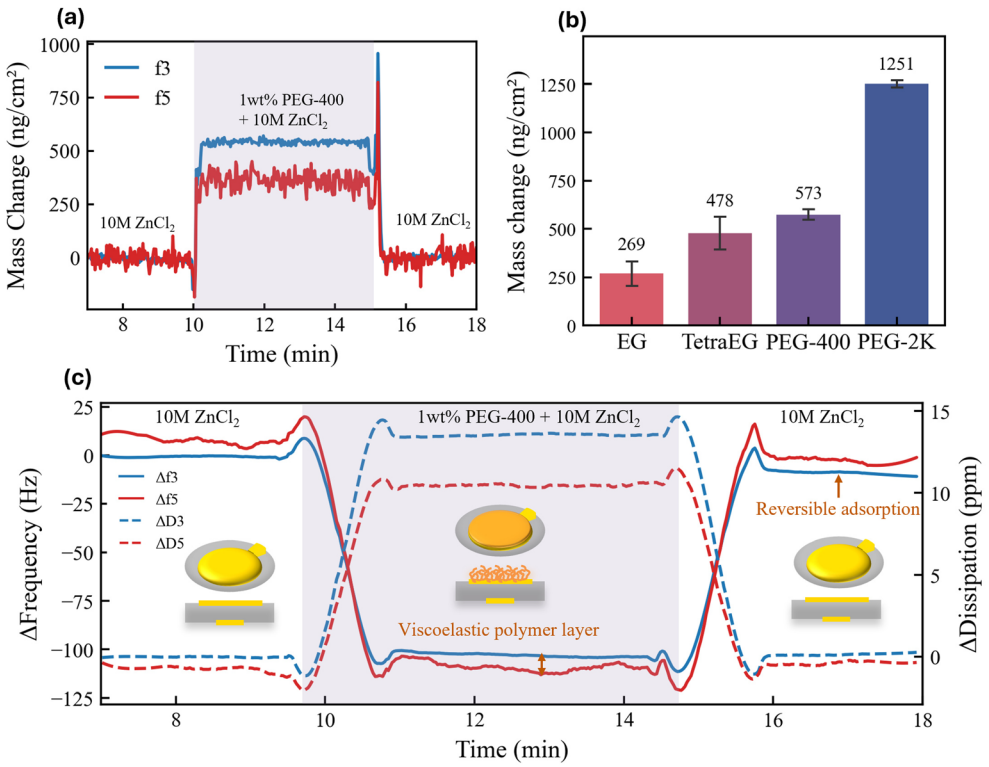

Fig. 3 QCM measurement of interfacial adsorption behavior. (a) Representative mass change over time during the QCM flow experiment. From 5–10 min, the electrolyte was 10 M $ZnCl_2$; from 10–15 min, 1 wt% PEG-400 in 10 M $ZnCl_2$ was flowed; and from 15–20 min, the electrolyte was switched back to 10 M $ZnCl_2$. Data are shown for both the 3rd (f3) and 5th (f5) harmonics. (b) Average mass change observed for 1 wt% EG-derived additives in 10 M $ZnCl_2$ under the same experimental format. Error bars represent the standard deviation across three independent experiments for each condition. (c) Raw frequency and dissipation data corresponding to the 3rd and 5th harmonics. Inset schematics represent QCM sensor surface over the period of the experiment.

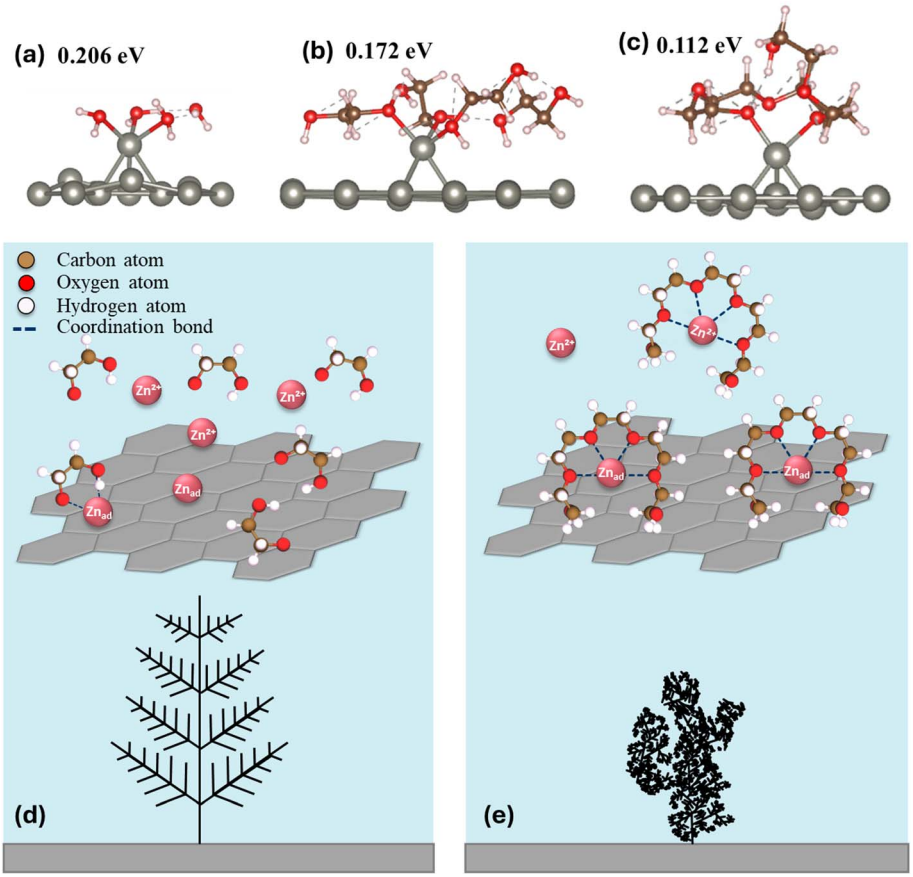

Fig. 4 Adsorbed EG-derived species shift dendrite growth mode. A Zn adatom on the Zn (002) surface stabilized by (a) four water molecules; (b) four EG molecules; (c) one Penta-EG molecule as simulated using DFT. The adatom binding energies are noted for each configuration. (d) In the presence of short-chain EG-derived molecules, weak coordination with Zn species at the interface permits classical continuous growth (CG) of dendrites. (e) By contrast, longer-chain oligomers exhibit stronger coordination with Zn species at the growth front, which suppresses continuous elongation and instead promotes independent nucleation (IN) of new crystallites.

with an average molecular weight M_w of 400. QCM-D measurements indicate that large amounts of EG-derived species adsorb on the electrode surface. This apparent discrepancy suggests that the "efficiency" of promoting the CG → IN transition decreases when the polymer chains become too long. DFT simulations of long-chain molecules are technically challenging due to the complexity of chain conformations and the large number of atoms required in the unit cell. It is well established that polymer chains can exhibit entanglement,[32] in which they overlap and interpenetrate in space once they exceed a critical chain length, defined by the entanglement molecular weight (M_e). When chains entangle with one another, many repeat units are consumed in chain–chain overlap rather than chain–metal surface interaction, weakening the effective polymer–metal binding. Interestingly, the M_e of PEG has been reported to be on the order of 10^3 g mol^{-1}.[33] We therefore theorize that the reduced efficiency of promoting CG → IN transition could arise from chain entanglement as the length increases.

^{1}H-NMR measurements provide a complementary perspective on how adsorbed EG-derived species influence dendrite growth modes. We recorded the ^{1}H-NMR spectra of 1 wt% EG-derived species dissolved in D_2O, both before and after adding $ZnCl_2$, to probe how interactions with ionic species alter the spectra (refer to Fig. S18 and S19 for alternative methods attempted). Notably, the magnitude of the peak shift reaches its maximum for PEG-400 (Fig. 5a) and decreases as the chain length increases. In particular, we tracked the ^{1}H-NMR signal corresponding to the proton labeled "c," which is bound to the backbone carbon atom (Fig. 5b). Representative spectra are shown on the right (Fig. 5c–e). The physical significance of the peak shift can be understood by considering its origin. A downfield (rightward) shift indicates increased shielding of the observed protons upon salt addition, which corresponds to an increase in local electron density.[34] This is consistent with hydrated Zn^{2+} ions coordinating with the electron-donating ether oxygens of the polymer backbone. To maintain charge neutrality, chloride anions would also be associated with the polymer vicinity.[35–37] A proposed molecular interaction scheme is illustrated in Fig. S20.[38] Therefore, the trend of peak shifts shown in Fig. 5a suggests that the strongest electronic interaction between Zn^{2+} cations and the EG-derived species is achieved with PEG-400. It is however important to note that the Zn^{2+} cations discussed here are distinct from the charge-neutral Zn^0 adatoms considered in the DFT calculations.

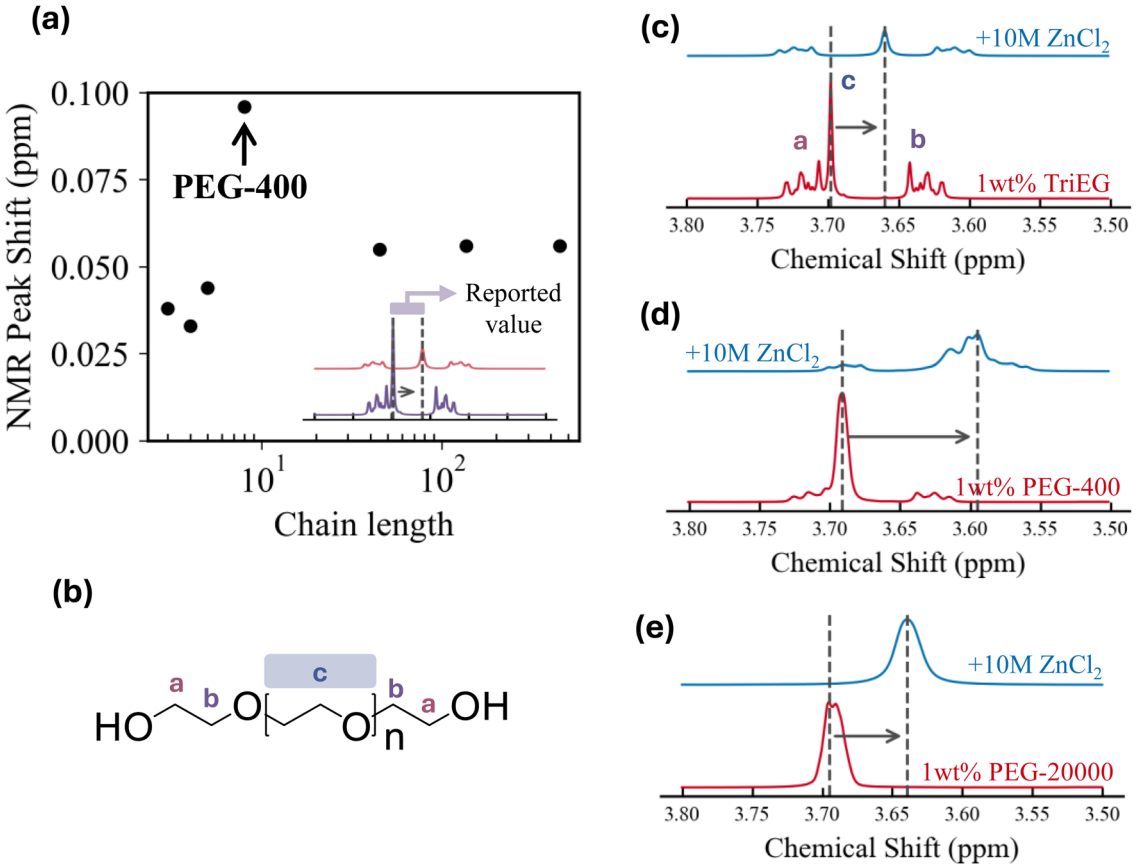

Fig. 5 ^{1}H-NMR measurement of chemical interactions between Zn^{2+} and EG-derived species. (a) Summary of ^{1}H-NMR peak shifts (decrease in chemical shift) upon addition of 10 M $ZnCl_2$ to 1 wt% polymer additive in D_2O. (b) Proposed peak assignment based on NMR results. (c–e) Representative NMR spectra for short-chain species, PEG-400, and long-chain species.

The role of the interaction between Zn^{2+} cations and EG-derived species can be speculated in the context of mass transport. The adsorbed polymer layer acts as a viscoelastic interphase covering the electrode surface. During electrodeposition, Zn^{2+} ions must migrate from the bulk electrolyte, across this interphase, to reach the crystal surface. Stronger Zn^{2+}–polymer interactions make this process kinetically less favorable, as each cation must dissociate from one –(CH_2CH_2O)– site before moving to the next, thereby slowing ion transport through the layer. An analogous negative correlation between interaction strength—for example, as reflected by the binding energy of the diffusing species to the substrate or medium—and diffusivity has been reported in a variety of systems.[39] When this interaction is maximized with PEG-400, ion transport across the adsorption layer to existing crystals is significantly hindered, making independent nucleation more favorable than continuous growth and rendering PEG-400 the most effective among EG-derived species in driving the CG → IN transition. This explanation is highly consistent with the trends observed in the QCM and NMR data; however, the presence of chain entanglement under the low polymer concentrations, highly saline conditions, and surface-confined environment used here cannot be experimentally confirmed and should therefore be regarded as a plausible but speculative mechanistic hypothesis.

In summary, based on QCM and NMR results, the reduced efficiency of the CG → IN transition observed with longer chains could be attributed to possible chain entanglement and their diminished effectiveness as Zn^{2+} transport barriers to existing crystals, compared with PEG-400.

Understanding impact on cell cycling

In order to understand the impact of growth morphology on cell cycling, the same *operando* cell set-up was used to study behavior over multiple plating and stripping cycles. The progression of the dendritic growth front towards the counter electrode was tracked over cycles as an additional metric to understand propensity of a growth morphology towards shorting behavior. Fig. 6a shows that growth Mode I: CG (1 wt% EG representative system) results in erratic and uneven dendrite growth, with the growth front advancing irregularly towards the counter electrode in consecutive cycles. This sporadic propagation suggests a high risk of an early short-circuit, as isolated dendrites can rapidly bridge the gap between electrodes.[40] In this mode, a short could potentially occur after only a few cycles due to the unpredictable leaps of the dendritic front. In contrast to this, with the growth Mode II: IN (1 wt% PEG-400 representative system) dendrite growth progresses in a uniform and controlled manner, with the growth front advancing at a nearly linear rate over successive cycles.

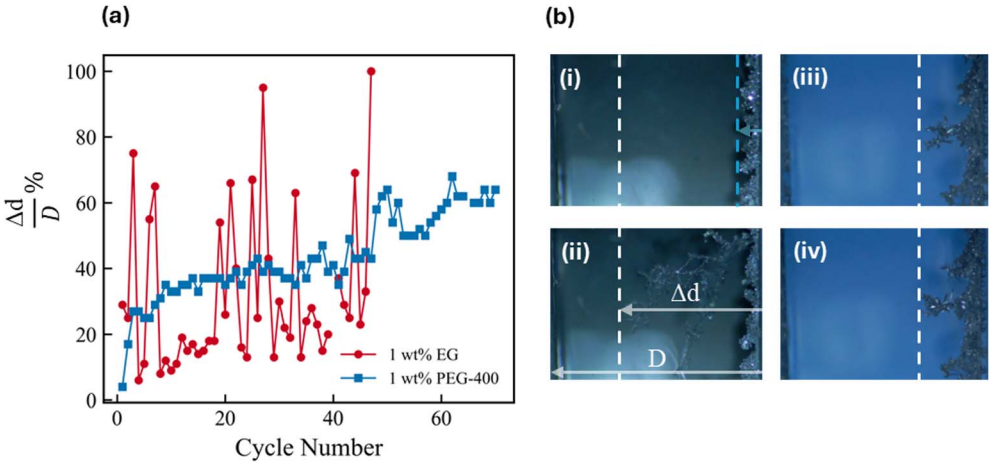

Fig. 6 Cycling performance monitored *via operando* visualization. (a) Normalized distance travelled by the dendritic growth front to the counter electrode at the end of each plating cycle. Δ*d* is the distance travelled by the dendritic growth front; *D* is the inter-electrode distance. (b) Representative *operando* visualization of dendritic growth front after consecutive plating cycles. (i) and (ii) 1 wt% EG system, Mode I growth. (iii) and (iv) 1 wt% PEG-400 system, Mode II growth. Conditions for plating-stripping cycles were at constant current of $J_{over\text{-}limiting}$ (861 mA cm^{-2}, 3 times the limiting current density of this system) and capacity of 15 mAh cm^{-2} with 1 wt% EG additive as representative for CG growth and with 1 wt% PEG-400 additive as representative for IN growth. Dashed white line shows the distance travelled in the second of the consecutive cycles.

Consequently, the propensity for dendrites to reach the counter electrode unpredictably is greatly reduced, translating to a lower short-circuit risk. Therefore, despite the uniform potential signature during cycling shown in Fig. S21, the *operando* visualization as demonstrated by Fig. 6b reveals improved predictability and cycle life with growth Mode II over growth Mode I. The erratic, unstable dendrite propagation observed in Mode I points to the heightened vulnerability of such morphologies under fast-charging conditions, where local overpotentials and concentration gradients are exacerbated often leading to dendritic growth. These insights are particularly valuable for the design of aqueous Zn batteries, where dendrite formation remains one of the key bottlenecks limiting practical charging rates and energy densities.[40]

Conclusion

The primary discovery of this work is that even trace amounts of EG-derived species (as low as 0.001 wt%, 10 ppm) can decisively govern the interfacial dynamics of diffusion-limited electrochemical crystallization. Adsorbed EG-derived species passivate Zn adatoms on existing crystals and create an energy barrier for Zn^{2+} transport through the viscoelastic interphase formed on the electrode surface. This interfacial dynamic suppresses continuous dendrite growth and instead promotes independent nucleation of new crystals with orientational correlation, driving the observed CG → IN transition. The transition is accompanied by a sixfold reduction in dendrite propagation rate, significantly improving electrochemical stability. We further show that the efficiency of this phenomenon is highly sensitive to polymer chain length, with PEG-400 ($n \approx 9$) achieving the strongest effect. Reduced efficiency at shorter or longer chain lengths arises from weaker adsorption or chain entanglement, leaving continuous growth more favorable. These findings open new directions, including electrochemical QCM-D under applied bias to quantify adsorption and molecular dynamics simulations to probe transport across the viscoelastic layer. Overall, the reported interfacial adsorption–induced CG → IN transition offers important implications for molecular-level design of electrolyte components for fast-charging electrochemical energy storage systems.

Author contributions

A. A. performed the electrochemical experiments and analyses. W. C. and G. H. conducted the DFT calculation. K. Z. directed the project.

Conflicts of interest

The authors declare no conflicts of interest.

Data availability

The data supporting this article have been included in the main text and supplementary information (SI) file. Supplementary information is available. See DOI: https://doi.org/10.1039/d5ta09175f.

Acknowledgements

The authors acknowledge financial support from the National Science Foundation (NSF) Materials Research Science and Engineering Center (MRSEC, DMR-2308817) and the University of Texas Science and Technology Acquisition and Retention (STARs) Fund. K. Z. gratefully acknowledges the membership of Allen J. Bard Center for Electrochemistry. The authors gratefully acknowledge the Allen J. Bard Center for Electrochemistry, University of Texas at Austin, for providing research support for

this work through the Bard CEC Instrumentation Facility maintained under grant no. H-F-0037 from the Welch Foundation. The authors thank the Texas Materials Institute for assisting in the physical characterization of the samples in this work. The authors acknowledge the Texas Advanced Computing Center (TACC) at The University of Texas at Austin for providing computational resources that have contributed to the research results reported within this paper. The authors also thank Prof. Venkat Ganesan, Prof. Venkat R. Subramanian, and Prof. Charles Buddie Mullins for many useful discussions.

References

1 R. Trivedi and W. Kurz, Dendritic growth, *Int. Mater. Rev.*, 1994, **39**(2), 49–74.
2 W. Kurz and D. J. Fisher, Dendrite growth at the limit of stability: tip radius and spacing, *Acta Metall.*, 1981, **29**(1), 11–20.
3 D. Barkey, F. Oberholtzer and Q. Wu, Kinetic anisotropy and dendritic growth in electrochemical deposition, *Phys. Rev. Lett.*, 1995, **75**(16), 2980.
4 B. P. Reis, R. P. França, J. A. Spim, A. Garcia, E. M. Da Costa and C. A. Santos, The effects of dendritic arm spacing (as-cast) and aging time (solution heat-treated) of Al–Cu alloy on hardness, *J. Alloys Compd.*, 2013, **549**, 324–335.
5 W. R. Osorio, P. R. Goulart, A. Garcia, G. A. Santos and C. M. Neto, Effect of dendritic arm spacing on mechanical properties and corrosion resistance of Al 9 Wt Pct Si and Zn 27 Wt Pct Al alloys, *Metall. Trans. A*, 2006, **37**(8), 2525–2538.
6 J. Zheng, J. Yin, D. Zhang, G. Li, D. C. Bock, T. Tang, Q. Zhao, X. Liu, A. Warren and Y. Deng, Spontaneous and field-induced crystallographic reorientation of metal electrodeposits at battery anodes, *Sci. Adv.*, 2020, **6**(25), eabb1122.
7 P. Bai, J. Li, F. R. Brushett and M. Z. Bazant, Transition of lithium growth mechanisms in liquid electrolytes, *Energy Environ. Sci.*, 2016, **9**(10), 3221–3229.
8 S. J. Banik and R. Akolkar, Suppressing dendrite growth during zinc electrodeposition by PEG-200 additive, *J. Electrochem. Soc.*, 2013, **160**(11), D519–D523.
9 D. A. Cogswell, Quantitative phase-field modeling of dendritic electrodeposition, *Phys. Rev. E*, 2015, **92**(1), 011301.
10 Y. Liu, X. Xu, M. Sadd, O. O. Kapitanova, V. A. Krivchenko, J. Ban, J. Wang, X. Jiao, Z. Song and J. Song, Insight into the critical role of exchange current density on electrodeposition behavior of lithium metal, *Advanced Science*, 2021, **8**(5), 2003301.
11 W.-Y. Jao, D. Sheyfer, J.-S. Micha, A. Aggarwal, H. Higdon, C.-C. Hu and J. X. K. Zheng, *Dendritic Growth in Battery Anodes: on the Hidden Role of Crystallographic Anisotropy at Propagating Electrochemical Interfaces*, 2025.
12 W. Shao and G. Zangari, Dendritic growth and morphology selection in copper electrodeposition from acidic sulfate solutions containing chlorides, *J. Phys. Chem. C*, 2009, **113**(23), 10097–10102.
13 M. A. Pasquale, L. M. Gassa and A. J. Arvia, Copper electrodeposition from an acidic plating bath containing accelerating and inhibiting organic additives, *Electrochim. Acta*, 2008, **53**(20), 5891–5904.
14 J. L. Ortiz-Aparicio, Y. Meas, G. Trejo, R. Ortega, T. W. Chapman and E. Chainet, Effects of organic additives on zinc electrodeposition from alkaline electrolytes, *J. Appl. Electrochem.*, 2013, **43**(3), 289–300.
15 M. Paunovic and M. Schlesinger, *Fundamentals of Electrochemical Deposition*, John Wiley & Sons, 2006.
16 S. K. Kim, D. Josell and T. P. Moffat, Electrodeposition of Cu in the PEI-PEG-Cl-SPS additive system: reduction of overfill bump formation during superfilling, *J. Electrochem. Soc.*, 2006, **153**(9), C616.
17 M. Tan and J. N. Harb, Additive behavior during copper electrodeposition in solutions containing Cl−, PEG, and SPS, *J. Electrochem. Soc.*, 2003, **150**(6), C420.
18 M. Kang and A. A. Gewirth, Influence of additives on copper electrodeposition on physical vapor deposited (PVD) copper substrates, *J. Electrochem. Soc.*, 2003, **150**(6), C426.
19 J. J. Kelly, C. Tian and A. C. West, Leveling and microstructural effects of additives for copper electrodeposition, *J. Electrochem. Soc.*, 1999, **146**(7), 2540.
20 S. J. Banik and R. Akolkar, Suppressing dendritic growth during alkaline zinc electrodeposition using polyethylenimine additive, *Electrochim. Acta*, 2015, **179**, 475–481.
21 K. R. Hebert, Role of chloride ions in suppression of copper electrodeposition by polyethylene glycol, *J. Electrochem. Soc.*, 2005, **152**(5), C283.
22 V. D. Jović and B. M. Jović, Copper electrodeposition from a copper acid baths in the presence of PEG and NaCl, *J. Serb. Chem. Soc.*, 2001, **66**(11–12), 935–952.
23 S. Wei, Z. Cheng, P. Nath, M. D. Tikekar, G. Li and L. A. Archer, Stabilizing electrochemical interfaces in viscoelastic liquid electrolytes, *Sci. Adv.*, 2018, **4**(3), eaao6243.
24 A. Warren, D. Zhang, S. Choudhury and L. A. Archer, Electrokinetics in Viscoelastic Liquid Electrolytes above the Diffusion Limit, *Macromolecules*, 2019.
25 Y. Jeon, Y. Wu, Y. Zhang, C. Hwang, H.-W. Lee, H.-K. Song and N. Liu, In situ visualization of zinc plating in gel polymer electrolyte, *Electrochim. Acta*, 2021, **391**, 138877.
26 A. Mitha, A. Z. Yazdi, M. Ahmed and P. Chen, Surface adsorption of polyethylene glycol to suppress dendrite formation on zinc anodes in rechargeable aqueous batteries, *ChemElectroChem*, 2018, **5**(17), 2409–2418.
27 G. S. Lindsay, D. Rohde, C. Wendeln, G. Vazhenin and A. A. Gewirth, Using SERS to Evaluate Additive Kinetics During Reverse Pulse Plating of Cu, *J. Electrochem. Soc.*, 2025, **172**(4), 042501.
28 M. L. Walker, L. J. Richter and T. P. Moffat, In situ ellipsometric study of PEG/Cl− coadsorption on Cu, Ag, and Au, *J. Electrochem. Soc.*, 2005, **152**(6), C403.
29 D. Johannsmann, A. Langhoff and C. Leppin, Studying soft interfaces with shear waves: Principles and applications of

the quartz crystal microbalance (QCM), *Sensors*, 2021, **21**(10), 3490.

30 A. D. Easley, T. Ma, C. I. Eneh, J. Yun, R. M. Thakur and J. L. Lutkenhaus, A practical guide to quartz crystal microbalance with dissipation monitoring of thin polymer films, *J. Polym. Sci.*, 2022, **60**(7), 1090–1107.

31 J. J. Kelly and A. C. West, Copper deposition in the presence of polyethylene glycol: I. Quartz crystal microbalance study, *J. Electrochem. Soc.*, 1998, **145**(10), 3472.

32 R. P. Wool, Polymer entanglements, *Macromolecules*, 1993, **26**(7), 1564–1569.

33 S. Y. Kim, H. W. Meyer, K. Saalwächter and C. F. Zukoski, Polymer dynamics in PEG-silica nanocomposites: effects of polymer molecular weight, temperature and solvent dilution, *Macromolecules*, 2012, **45**(10), 4225–4237.

34 H. Günther, *NMR Spectroscopy: Basic Principles, Concepts and Applications in Chemistry*, John Wiley & Sons, 2013.

35 G.-K. Liu, S. Zou, D. Josell, L. J. Richter and T. P. Moffat, SEIRAS study of chloride-mediated polyether adsorption on Cu, *J. Phys. Chem. C*, 2018, **122**(38), 21933–21951.

36 Z. V. Feng, X. Li and A. A. Gewirth, Inhibition due to the interaction of polyethylene glycol, chloride, and copper in plating baths: a surface-enhanced Raman study, *J. Phys. Chem. B*, 2003, **107**(35), 9415–9423.

37 Y. Wu, Z. Mao, T.-W. Jiang, X.-Y. Ma, L. Zheng, K. Jiang and W.-B. Cai, Revisiting the polyethylene glycol-chloride adsorption structure on Cu electrode in sulfuric acid solution by wide-frequency ATR-SEIRAS, *J. Phys. Chem. C*, 2023, **127**(44), 21695–21703.

38 S. Jin, J. Yin, X. Gao, A. Sharma, P. Chen, S. Hong, Q. Zhao, J. Zheng, Y. Deng and Y. L. Joo, Production of fast-charge Zn-based aqueous batteries *via* interfacial adsorption of ion-oligomer complexes, *Nat. Commun.*, 2022, **13**(1), 2283.

39 C. D. Geary, I. Zudans, A. V. Goponenko, S. A. Asher and S. G. Weber, Electrochemical investigation of Pb2+ binding and transport through a polymerized crystalline colloidal array hydrogel containing benzo-18-crown-6, *Anal. Chem.*, 2005, **77**(1), 185–192.

40 Y.-y. Zuo, K.-l. Wang, P.-c. Pei, M.-h. Wei, X.-t. Liu, Y. Xiao and P.-f. Zhang, Zinc dendrite growth and inhibition strategies, *Mater. Today Energy*, 2021, **20**, 100692.